

# Activation of p53: How phosphorylated Ser15 triggers sequential phosphorylation of p53 at Thr18 by CK1 $\delta$

Sonia T. Nicolaou<sup>1,2</sup>  | Srinivasaraghavan Kannan<sup>2</sup>  | Jim Warwicker<sup>1</sup>  |  
Chandra S. Verma<sup>2,3,4</sup> 

<sup>1</sup>Faculty of Biology, Medicine and Health,  
School of Biological Sciences, Manchester  
Institute of Biotechnology, University of  
Manchester, Manchester, UK

<sup>2</sup>Bioinformatics Institute, Agency for Science,  
Technology, and Research (A\*STAR),  
Singapore, Singapore

<sup>3</sup>School of Biological Sciences, Nanyang  
Technological University, Singapore, Singapore

<sup>4</sup>Department of Biological Sciences, National  
University of Singapore, Singapore, Singapore

## Correspondence

Chandra S. Verma, Bioinformatics institute,  
Agency for Science, Technology, and Research  
(A\*STAR), Singapore 138671, Singapore  
Email: [chandra@bii.a-star.edu.sg](mailto:chandra@bii.a-star.edu.sg)

## Funding information

Agency for Science, Technology and Research  
(A\*STAR); University of Manchester

## Abstract

The N-terminal transactivation domain (TAD) of p53 is a disordered region with multiple phosphorylation sites. Phosphorylation at Thr18 is crucial for the release of p53 from its negative regulator, MDM2. In stressed cells, CK1 $\delta$  is responsible for phosphorylating Thr18, but requires Ser15 to be phosphorylated. To understand the mechanistic underpinnings of this sequential phosphorylation, molecular modeling and molecular dynamics simulation studies of these phosphorylation events were carried out. Our models suggest that a positively charged region on CK1 $\delta$  near the adenosine triphosphate (ATP) binding pocket, which is conserved across species, sequesters the negatively charged pSer15, thereby constraining the positioning of the rest of the peptide, such that the side chain of Thr18 is positioned close to the  $\gamma$ -phosphate of ATP. Furthermore, our studies show that the phosphorylated p53 TAD1 (p53pSer15) peptide binds more strongly to CK1 $\delta$  than does p53. p53 adopts a helical structure when bound to CK1 $\delta$ , which is lost upon phosphorylation at Ser15, thus gaining higher flexibility and ability to morph into the binding site. We propose that upon phosphorylation at Ser15 the p53 TAD1 peptide binds to CK1 $\delta$  through an electrostatically driven induced fit mechanism resulting in a flanking fuzzy complex.

## KEY WORDS

fuzzy complex, intrinsically disordered proteins, molecular dynamics, p53, phosphorylation

## 1 | INTRODUCTION

Proteins are essential components of the living cell whose functionality is highly controlled by post-translational modifications (PTMs). Intrinsically disordered proteins and regions of proteins (simply referred to as IDPs) lack a fixed three-dimensional (3D) structure and instead exist as dynamic ensembles of interchanging conformations.<sup>1–5</sup> PTM sites are enriched in IDPs, and due to their flexible nature, they are easily accessible to modifying enzymes.<sup>6</sup> Phosphorylation is one of the most common PTMs and phosphorylation sites are typically found in disordered regions.<sup>7</sup> During a

phosphorylation event, the neutral side chain –OH group of a Ser, Thr, or Tyr residue is modified to a negatively charged  $\text{PO}_4^{2-}$  group by the transfer of a phosphate from an adenosine triphosphate (ATP) molecule bound to a protein kinase. The increase in negative charge from the addition of a phosphate group alters the steric, electrostatic, and hydrophobic properties of the protein, as well as its ability to interact with binding partners and thus is considered an important regulatory mechanism amongst eukaryotic processes,<sup>6,8,9</sup> and to a lesser extent in prokaryotes.<sup>10</sup>

Tumor suppressor p53 is a transcription factor with ordered and disordered regions and serves as a hub in protein–protein interaction

This is an open access article under the terms of the [Creative Commons Attribution](#) License, which permits use, distribution and reproduction in any medium, provided the original work is properly cited.

© 2022 Bioinformatics Institute. *Proteins: Structure, Function, and Bioinformatics* published by Wiley Periodicals LLC.

networks. It includes two large intrinsically disordered regions with multiple phosphorylation sites: an N-terminal transactivation domain (TAD) and a C-terminal regulatory domain.<sup>11</sup> Nine out of the more than 20 phosphorylation sites in p53 are located in TAD.<sup>12</sup> The TAD is divided into two subdomains: TAD1 (residues 1–40) and TAD2 (residues 41–61). In unstressed cells, TAD1 interacts with E3 ubiquitin ligase MDM2, keeping p53 levels low through continuous proteasomal degradation.<sup>13–15</sup> Upon stress, a series of PTM events (mainly phosphorylation) are initiated, activating p53 by releasing it from MDM2. Free p53 is stabilized by CBP/p300 and is able to accumulate in cells and turn on the transcription of genes that suppress tumor activity.<sup>16,17</sup> Disordered TAD1 interacts with both MDM2 and CBP/p300 (TAZ1 and TAZ2 domains) and forms an amphipathic helix in the bound state.<sup>12,18</sup>

Phosphorylation at Thr18 is crucial for the release of p53 from MDM2.<sup>19</sup> This phosphorylation is carried out by casein kinase 1 $\delta$  (CK1 $\delta$ ).<sup>20</sup> The protein kinase CK1 family comprises a set of highly similar Ser/Thr kinases involved in regulating a variety of cellular functions including but not limited to the circadian rhythm, cellular response to DNA damage, and apoptosis.<sup>21</sup> CK1 substrates often contain acidic or phosphorylated residues with a consensus sequence of pSer/pThr-X-X-(X)-Ser/Thr, where pSer/pThr are phosphorylated Ser or Thr (this position can also be occupied by an acidic residue), X represents any amino acid, and (X) represents a possible third residue.<sup>22,23</sup> Consistent with the sequence motif recognized by CK1, efficient phosphorylation of Thr18 in TAD1 requires prior phosphorylation at Ser15.<sup>20</sup> Although p53 has been extensively studied over the years, mechanisms that underpin several functions of p53 still remain unknown, including why Ser15 phosphorylation is a prerequisite for Thr18 phosphorylation.

IDPs frequently fold upon binding to their binding partners, a phenomenon known as coupled folding and binding.<sup>24</sup> This either occurs through conformational selection, where the bound-state-like structure of the IDP is present in the unbound state ensemble of conformations, or through induced fit, where the IDP folds into the desired state after the initial interaction with its binding partner.<sup>25–27</sup> Often, IDPs bind to their partners through a combination of the two mechanisms. However, some IDPs remain disordered even after binding and form fuzzy complexes.<sup>28</sup> Fuzzy complexes are divided into four structural categories: polymorphic, clamp, flanking, and random. Complexes are referred to as polymorphic when at least one of the partners adopts a few alternative structures (two in the simplest case).<sup>28,29</sup> Clamp complexes are formed when only the N- and C-termini of the IDP interact with a partner, while the linker remains disordered due to a lack of permanent contacts.<sup>28</sup> Flanking complexes on the other hand contain a short recognition motif within the linker region that is used for binding to the partner protein, while the termini of the IDP retain their conformational variability.<sup>28,29</sup> In random complexes, IDPs only interact with their partners through transient contacts and binding does not induce the formation of any secondary structure.<sup>28,29</sup> It is likely that the complex between the p53 TAD1 peptide and CK1 $\delta$  falls into one of these categories.

To examine the effect of Ser15 phosphorylation on the dynamics of the p53 TAD1 peptide (henceforth referred to as p53 peptide) and its recognition by the kinase, we studied the conformational dynamics of a free p53 peptide as well as a p53 peptide in complex with CK1 $\delta$ , in the presence and absence of Ser15 phosphorylation. In this study, the technique of accelerated molecular dynamics (aMD) was used to ensure comprehensive sampling of the conformational states of the systems.<sup>30</sup> Our results suggest that the increase in negative charge due to Ser15 phosphorylation leads to high conformational flexibility in the p53 peptide in both its free and bound states. This enables the peptide to dock such that phosphorylated Ser15 is sequestered in a positively charged region of the kinase which then holds the remaining peptide, thus localizing Thr18 to the vicinity of the ATP with its hydroxyl oriented in position to accept the incoming phosphate from ATP. In the bound state, the p53pSer15 peptide loses its helical structure, whereas the p53 peptide remains partly helical even in the bound state. We speculate that the phosphorylated p53 peptide binds CK1 $\delta$  through an induced fit mechanism to form a fuzzy complex.

## 2 | MATERIALS AND METHODS

### 2.1 | System preparation for free p53 peptides

An initial fully extended p53 TAD1 peptide, residues 9–24, without phosphorylation, was built using the xleap module of the AmberTools<sup>19</sup><sup>31</sup> package to avoid bias from bound structures. The N- and C-termini of the peptide were capped with acetyl and N-methyl groups, respectively.

### 2.2 | System preparation for p53 peptides bound to CK1 $\delta$

The experimental structure of CK1 $\delta$  was obtained from the Protein Data Bank (PDB id 6ru6; resolution 2.05 Å)<sup>32,33</sup> and all the crystallographic waters were retained. The binding pose of the peptide to CK1 $\delta$  was taken from Protein Data Bank structure 6ru7, that includes a p63 peptide (resolution 2.08 Å).<sup>32</sup> ATP and two complexed Mg<sup>2+</sup> ions were added using Protein Data Bank entry 3x2w (resolution 1.7 Å)<sup>34</sup> by superimposing the protein structures using PyMOL.<sup>35</sup> Modeller<sup>36</sup> was used to fill missing residues in the structure 6ru6. The C-terminus of CK1 $\delta$  was capped using an N-methyl cap. The likely protonation states of hydrogens in the 6ru6 structure were generated using the programs MolProbity<sup>37</sup> and PDB2QR.<sup>38</sup> Two different p53 TAD1 peptides, residues 9–24, (a) without phosphorylation and (b) with Ser15 phosphorylation, bound to CK1 $\delta$  with Thr18 residue placed adjacent to ATP, were created by mutating the peptide residues from PDB structure 6ru7 to p53 residues using PyMOL. The mutated peptides were added to the 6ru6 structure by superimposing them using PyMOL. The N- and C-termini of the peptides were capped with acetyl and N-methyl groups, respectively.

### 2.3 | System preparation for mutant CK1 $\delta$ complexes

The following residues of CK1 $\delta$  in both the p53 and p53pSer15 complexes were mutated to Ala: Arg98, Lys130, Arg178, Lys221, Arg222, and Lys224. Mutations were determined from alanine scanning calculations. Since we were interested in the dominant interactions that the negatively charged peptide (due to phosphorylated Ser15) makes with the kinase, only the positively charged residues that contributed most to binding were mutated. PyMOL was used to perform the mutations to Ala.

### 2.4 | Molecular dynamics simulations of free peptides

The linear free p53 peptide structure without phosphorylation was used as the starting structure for this study. Implicit solvent molecular dynamics (MD) simulations were carried out to collapse the extended structure created with xleap to reduce the size of the water box. The behavior of peptides in solution is simulated by immersing them in a box of water molecules and carrying out MD simulations. However, the extended structures of the peptides require a large water box and to reduce the associated computational costs, we initially subject the peptides to implicit solvent MD simulations to collapse their conformations, thereby requiring smaller boxes of water molecules for explicit solvent MD simulations.<sup>39</sup> The sander module of the Amber11<sup>40</sup> package was used for energy minimization and equilibration of the system with the Amber ff14SB<sup>41</sup> force field. A 1500 step minimization was initially conducted, followed by gradual heating of the system from 0 to 300 K over 80 ps. This was followed by further heating of the system from 300 to 450 K over 5 ns in order to enhance conformational sampling. A production simulation at 300 K was carried out over 0.5 ns using pmemd, the CUDA module of Amber18.<sup>42</sup>

Next, the xleap module of AmberTools19 was used to prepare the system for explicit solvent MD simulations using the implicit solvent production model as the starting structure. The system was solvated in an octahedral box using the TIP3P water model,<sup>43</sup> with at least 10 Å separating the solute atoms and the edges of the box. Counter ions were added to neutralize the system. Energy minimization and equilibration simulations were carried out using the sander module of the Amber11 package with the ff14SB force field. A 10 000 step energy minimization of the system was carried out, with positional restraints on the peptide (force constant: 5 kcal/molÅ<sup>-2</sup>), allowing the solvent and ions to move freely. This was followed by a 10 000 step minimization of the system without positional restraints on the peptide atoms, to remove steric clashes.<sup>44</sup> The system was gradually heated from 0 to 300 K with positional restraints on the peptide (force constant: 25 kcal/molÅ<sup>-2</sup>) over 40 ps. Once the system reached 300 K, the positional restraints were gradually removed over 50 ps, and the system was equilibrated for another 100 ps without any positional restraints at 300 K, at constant pressure. A time

constant of 0.1 ps was used for heat bath coupling for the system. The particle mesh Ewald (PME) method with a 9 Å real space cutoff was used to treat long-range electrostatic interactions.<sup>45</sup> The SHAKE algorithm was used to constrain bonds involving hydrogens.<sup>46</sup> The resulting structures were used as the starting structures for production MD simulations. Production MD simulations were carried out for 500 ns in triplicates using pmemd, the CUDA module of Amber18. The same protocol for system preparation, minimization, equilibration, and production procedures was used for the phosphorylated peptide. The parameters for phosphorylated serine were taken from Homeyer et al.<sup>47</sup>

### 2.5 | MD simulations of CK1 $\delta$ complexes

The xleap module of AmberTools19 was used to prepare the CK1 $\delta$  complexes for explicit solvent MD simulations. A three-step minimization was carried out for the protein-peptide complexes using the sander module of the Amber11 package with the ff14SB force field. First, a 10 000 step energy minimization of the system was carried out, with positional restraints on the kinase and peptide (force constant: 5 kcal/molÅ<sup>-2</sup>) allowing ATP, the Mg<sup>2+</sup> ions, solvent, and counterions to move freely. The second step of minimization was carried out over an additional 10 000 steps, this time with restraints on the kinase only (force constant: 5 kcal/molÅ<sup>-2</sup>), allowing the peptide, ATP, solvent, and ions to move freely. This was followed by a third 10 000 step minimization of the system without positional restraints, to remove steric clashes. The system was gradually heated from 0 to 300 K with positional restraints on the whole system (force constant: 25 kcal/molÅ<sup>-2</sup>) over 40 ps. Once the system reached 300 K, the positional restraints were gradually removed over 50 ps, and the system was equilibrated for another 100 ps without any positional restraints at 300 K, at constant pressure. The PME method with a 9 Å real space cutoff was used to treat long-range electrostatic interactions.<sup>45</sup> A time constant of 0.1 ps was used for heat bath coupling for the system. The SHAKE algorithm was used to constrain bonds involving hydrogens.<sup>46</sup> The resulting structures were used as the starting structures for production MD simulations. Production MD simulations for 1  $\mu$ s were carried out in triplicates using pmemd, the CUDA module of Amber18.

### 2.6 | Accelerated MD simulations

Accelerated MD (aMD) was used in order to enhance conformational sampling of the systems, by adding a robust bias potential to the potential energy of the system in order to lower the height of local energy barriers between minima to allow the simulation to progress at a faster pace.<sup>30</sup> In this study, dual-boost aMD simulations were performed with boost energies added in both the total potential energy and the dihedral energy. The structures from explicit solvent production MD simulations for free peptides (after 500 ns) and CK1 $\delta$  complexes (after 100 ns; described in the previous section) were used as



starting structures for aMD. All simulations were carried out in explicit solvent at 300 K using the pmemd module of Amber18. For free peptides, production simulations were carried out for 250 ns, and for protein-peptide complexes production simulations were carried out for 500 ns. The same protocol was followed for production simulations of the mutant CK1 $\delta$  complexes.

The convergence of the systems was evaluated by dividing the aMD trajectories into five equal segments and calculating the root mean square deviation (RMSD) of each segment using the first frame as reference. For the free peptide simulations, the initial aMD trajectories were divided into 50 ns segments, and for the bound peptides the trajectories were divided into 100 ns segments. Since both systems are intrinsically disordered the RMSD distribution plots have multiple peaks that represent different conformations, but the number of peaks decreases as a function of time, suggesting convergence (Figure S1A-D).

## 2.7 | Binding energy calculations, energy decomposition, and alanine scanning

Molecular mechanics generalized born surface area and molecular mechanics Poisson Boltzmann surface area (MMPBSA) methods were used to calculate the binding free energies of the peptides to the kinase.<sup>49,50</sup> Binding free energies were calculated for each protein-peptide complex simulation. The effective binding energies were decomposed into contributions of individual residues using the MMPBSA energy decomposition method. The last 250 ns of the trajectories were used, sampling every 100 frames. Mbondi2 radii were used for these calculations.

Alanine scanning calculations were carried out to determine the residues within the kinase that contribute the most to binding to the peptides. Residues of the kinase that were located within 6 Å of the peptide were mutated to alanine with the exception of glycine. The polar contribution to the solvation free energy was calculated by using the generalized born method (igb = 5).

## 2.8 | Two-dimensional free energy surfaces

Two-dimensional free energy surfaces (2DFESs) were plotted for the characterization of peptide energy landscapes from our simulations. The reaction coordinates selected were (i) radius of gyration ( $R_g$ ) of free peptide/peptide in the complex and (ii) end-to-end distance of free peptide/peptide in the complex.

## 2.9 | Analysis

The cpptraj module of Amber18<sup>51</sup> was used to calculate RMSD,  $R_g$ , root mean square fluctuation (RMSF), solute-solute and solute-solvent hydrogen bond interactions, secondary structure using the DSSP method,<sup>52</sup> end-to-end distance (measured between center of mass of the capping residues), distance between the  $\gamma$ -phosphate of

ATP and the side chain hydroxyl group of Thr18, and k-means clustering. For the free peptide simulations, the first 100 ns were excluded from analysis for both normal and accelerated MD. For the aMD complex simulations, only the last 250 ns were considered. Visual molecular dynamics (VMD)<sup>53</sup> and PyMOL<sup>35</sup> were used for visualization of the simulations.

## 3 | RESULTS

### 3.1 | Conformational dynamics of free p53 peptides in solution

p53 TAD1 is highly dynamic and is known to adopt a helical conformation when bound to the hydrophobic pocket of MDM2 (PDB id 1YCR).<sup>54</sup> In this work, the conformational dynamics of free p53 peptides in solution were explored by using the enhanced sampling method, aMD. Simulations of free peptides with and without phosphorylation were stable in solution. Due to the flexible nature of the free p53 peptides absolute convergence is not expected. However, examination of the RMSD distributions over 50 ns windows shows that the number of peaks (representing different conformational clusters) decrease over time for both unphosphorylated and phosphorylated peptides (Figure S1A,C), suggesting convergence. RMSD as a function of time (Figure S1E, F) again demonstrates convergence although the free peptides appear to occupy alternating minima in a pseudo-periodic manner (Figure S1E).

The p53 and p53pSer15 peptides have similar  $R_g$  values ranging from 6 to 11 Å and from 6 to 12 Å, respectively. However, p53 has a broader peak at 8 Å whereas p53pSer15 has a narrower peak around 7.5 Å indicating a preference for slightly more expanded conformations in the unphosphorylated state (Figure 1A). The end-to-end distance distribution of p53 has a peak value around 20 Å while p53pSer15 peaks at 15 Å, values that are in line with observations from  $R_g$  (Figure 1C).  $R_g$  and end-to-end distance calculations suggest that p53 samples more extended conformations relative to p53pSer15. The 2DFESs plots for free peptides in solution were created with  $R_g$  on the x-axis and end-to-end distance on the y-axis. The p53 peptide has a large local energy minimum with an  $R_g$  value that spans from 8 to 9 Å and end-to-end distances range from 17 to 28 Å. The p53pSer15 peptide has an energy minimum with an  $R_g$  at 7.5 Å and an end-to-end distance between 10 and 17 Å (Figure 2A,B). The 2D energy surface analysis once more shows that the free p53 peptide is more extended in solution compared with p53pSer15.

### 3.2 | Free p53 peptide retains helicity after Ser15 phosphorylation

The p53 peptide samples more helical conformations (41%) compared with p53pSer15 (37%). Helical conformations ( $\alpha$  and  $3_{10}$ ) are

**FIGURE 1** Distributions of radius of gyration ( $R_g$ ) and end-to-end distances for p53 and p53pSer15 peptides in their free and bound forms using Kernel Density Estimation (KDE). (A,C) Free peptide distributions. (B,D) Bound peptide (to CK1 $\delta$ ) distributions. p53 peptide distributions are colored in blue and p53pSer15 in orange.

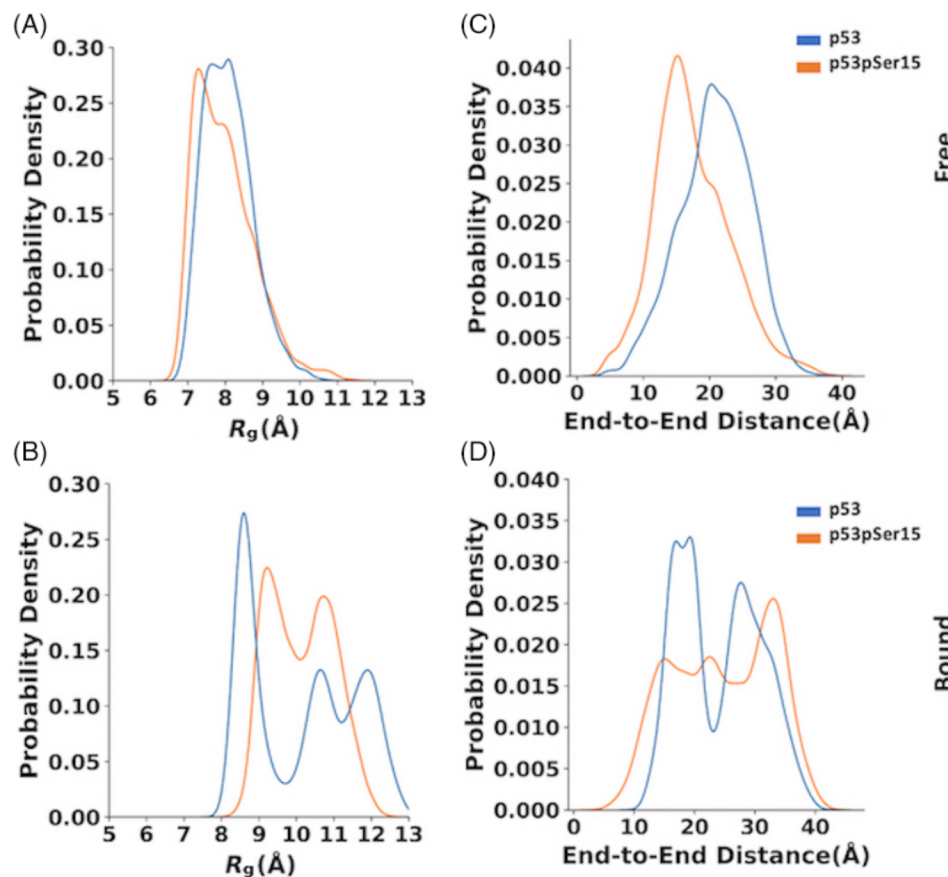
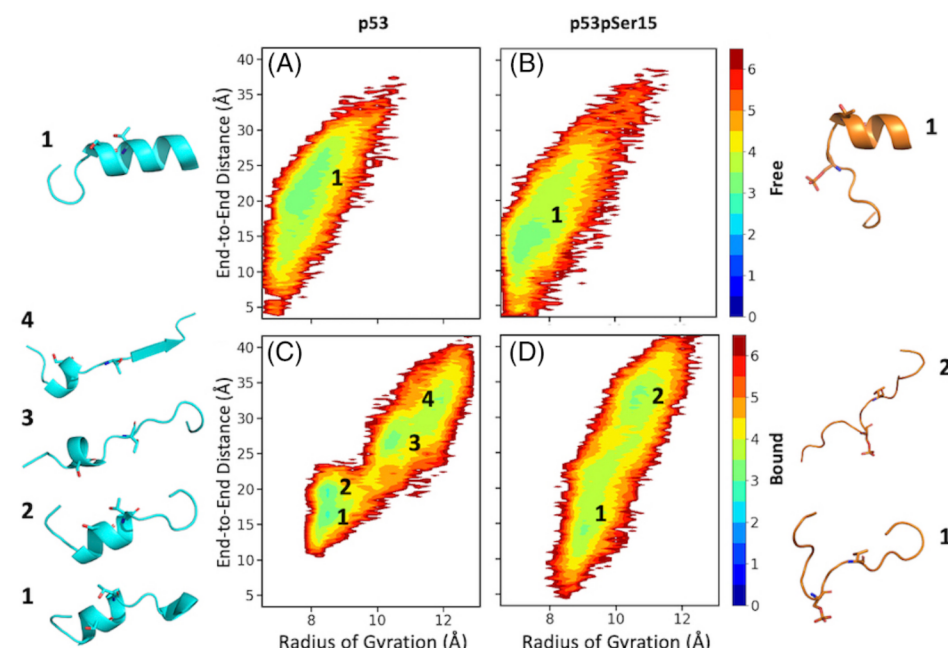


**FIGURE 2** Two-dimensional free energy landscape of free and bound p53 and p53pSer15 peptides as a function of radius of gyration ( $R_g$ ) and end-to-end distance. Panel (A) corresponds to conformations of the free p53 peptide. Panel (B) corresponds to conformations sampled in the free p53pSer15 peptide simulations. Panels (C,D) correspond to p53 and p53pSer15 peptide conformations bound to casein kinase 1 $\delta$ , respectively. Representative conformations from each energy minimum are shown on the left and right sides of the plots and are numbered accordingly, with Ser15 and Thr18 residues shown as sticks.



observed from residues Leu14 to Lys24 of p53 and Gln16 to Lys24 in p53pSer15 (Figure 3A,B,E). Ser15 is 33% helical in p53 and drops to 11% in p53pSer15. Phosphorylation at Ser15 affects helicity around the site as the negatively charged phosphate group prefers to be solvated, but the peptide maintains its helicity along the rest

of the chain. Interactions from  $i$  to  $i + 4$  were observed between backbone residues of Ser15-Phe19 (48%), side chain and backbone residues of Leu14-Thr18 (25% and 18%), and backbone residues of Thr18-Leu22 (23%) in p53. The presence of the negatively charged phosphate results in attenuation of the hydrogen bonding



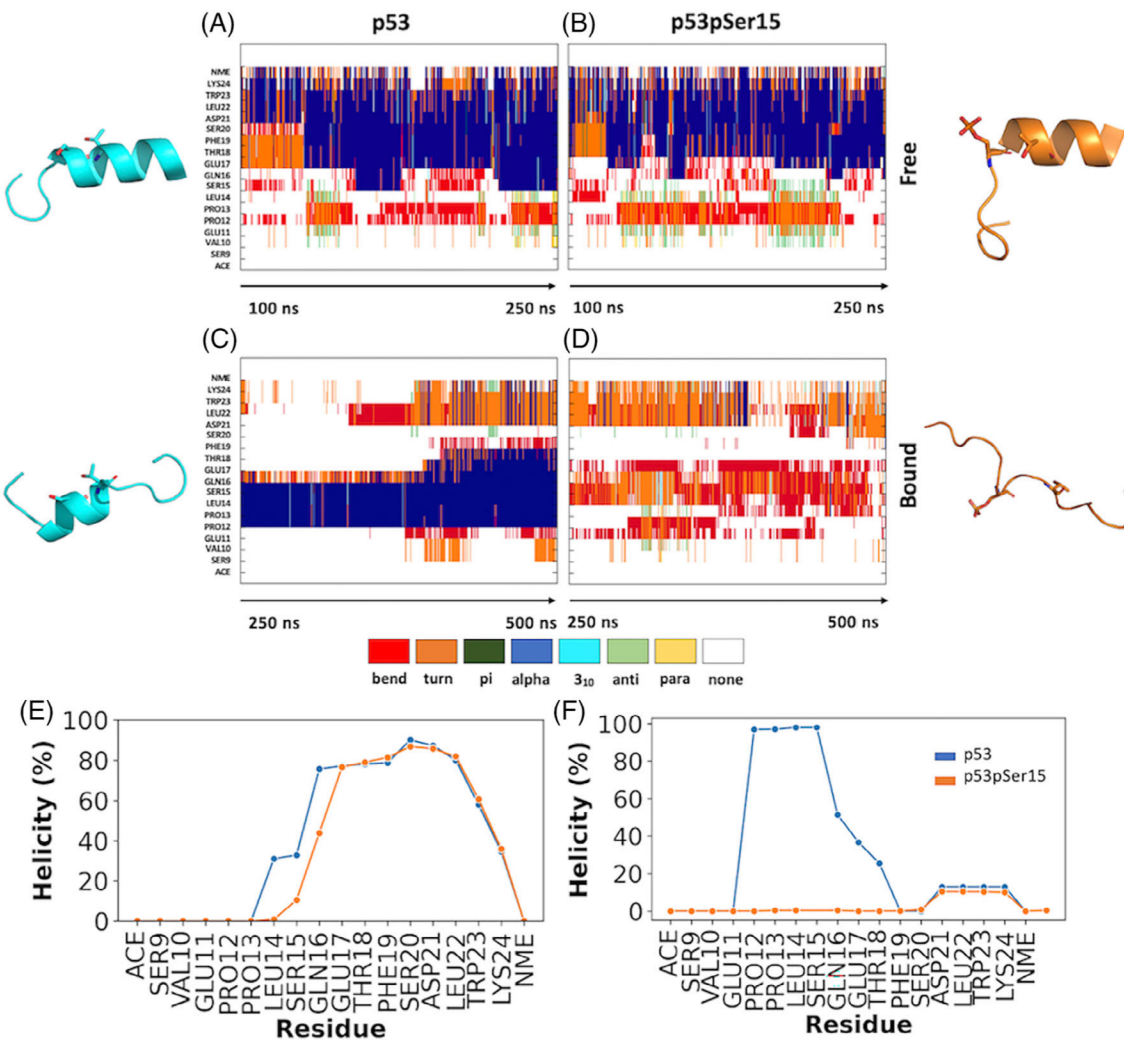


**FIGURE 3** Secondary structure determination for p53 and p53pSer15 peptides in the free and bound states from accelerated molecular dynamics simulations. (A,B) Secondary structure per residue as a function of time (0.01 ns/frame) for free p53 and p53pSer15 peptides. (C,D) Secondary structure per residue as a function of time for p53 and p53pSer15 peptides bound to casein kinase 1 $\delta$ . (E,F) Average percent helicity per residue in free and bound p53 and p53pSer15 peptides. p53 peptide is represented in blue and p53pSer15 peptide in orange.

interactions between the backbone of Ser15-Phe19 (27%) and side chain of Leu14-Thr18 (8%), whereas the Thr18-Leu22 hydrogen bond interaction is not affected (22%).

### 3.3 | Conformational dynamics of p53 peptides bound to CK1 $\delta$ in solution

We next investigated the conformations sampled by the peptides when bound to CK1 $\delta$ . Initial benchmark simulations of the modified crystal structure (data not shown) were carried out to test the stability of the complex with the selected force field. The complexes were stable using the ff14SB force field.<sup>42</sup> The conformational dynamics of the p53 peptides with and without phosphorylation bound to CK18 were studied using aMD. The convergence of the systems was evaluated by looking at their RMSD distributions as well as their RMSD with respect to time. The number of peaks in the RMSD distribution

plot decrease over the simulation time suggesting convergence (Figure S1B,D). RMSD with respect to time indicates that while the systems are dynamic, they are mostly stable after the first 250 ns and undergo smaller motions compared with the free peptides (as expected; Figure S1F).

The range of  $R_g$  values for the bound p53 peptide from aMD simulations was between 7.5 and 13 Å with a major peak around 8.5 Å. The bound p53pSer15 peptide ranged from 8 to 13 Å with peaks around 9 and 11 Å (Figure 1B). The large  $R_g$  values signify that the phosphorylated peptide is more expanded than the unphosphorylated in the bound state. The same pattern is observed from end-to-end distance calculations for both the unphosphorylated and phosphorylated peptides. p53 has two broad peaks around 15 and 30 Å and p53pSer15 has a peak at 35 Å (Figure 1D). Free energy surface plots show that the p53 peptide has four local energy minima: one with an  $R_g$  value around 8.5 Å and an end-to-end distance of 15 Å, a second minimum with  $R_g$  value around 8.5 Å and an end-to-end distance of

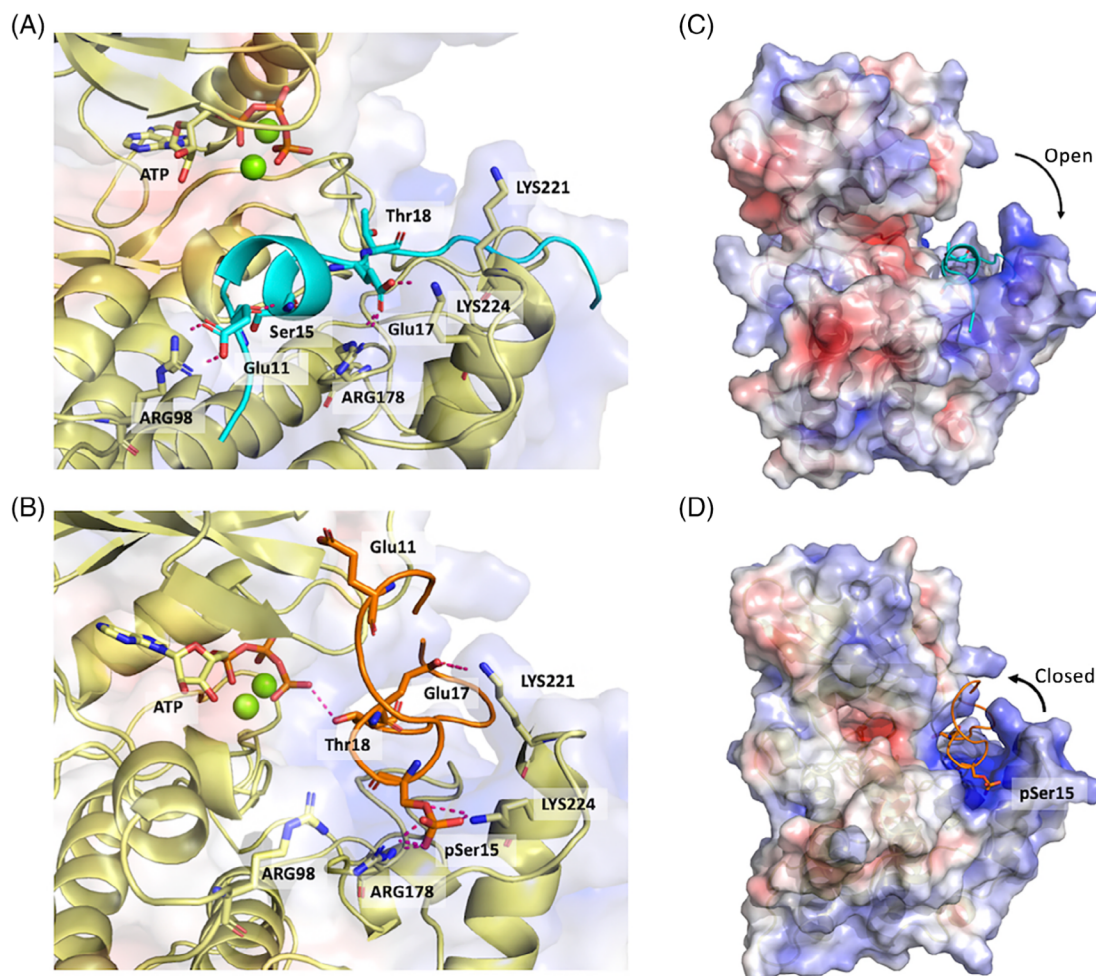


**FIGURE 4** Structural basis for the binding of p53 peptides with and without phosphorylation on casein kinase 1 $\delta$  (CK1 $\delta$ ). (A,B) CK1 $\delta$  (yellow cartoon, transparent electrostatic surface) in complex with p53 (cyan) and p53pSer15 (orange). Protein-peptide H-bond interactions within the binding pocket are represented by dashed lines. Mg<sup>2+</sup> ions are shown as green spheres and adenosine triphosphate is shown in sticks. (C,D) Electrostatic potential surface of CK1 $\delta$  (blue/red for positive/negative charge) in complex with p53 peptide is shown in cyan and p53pSer15 peptide is shown in orange.

20 Å, a third energy minimum with an  $R_g$  value at 10.5 Å and an end-to-end distance around 26 Å, and a fourth smaller minimum with an  $R_g$  at 12 Å and an end-to-end distance between 30 and 35 Å (Figure 2C). The free energy surface plot of p53pSer15 shows that there is a small local minimum with an  $R_g$  value at 9 Å and an end-to-end-distance value around 14 Å and a second larger energy minimum with an  $R_g$  at 11 Å and an end-to-end distance between 30 and 35 Å (Figure 2D). The shift in local energy minima shows that phosphorylation causes the peptide to sample more extended conformations compared with the unphosphorylated peptide.

### 3.4 | CK1 $\delta$ bound p53 peptide loses helicity when Ser15 is phosphorylated

The p53 favors more collapsed conformations than bound p53pSer15 when complexed to CK1 $\delta$ . Secondary structure analysis of the bound peptides from aMD simulations shows that in addition to being more

collapsed, the p53 peptide is more helical compared with p53pSer15. Phosphorylation at Ser15 destabilizes the helix observed in p53 and leads to a less structured peptide (Figure 3C,D,F). p53 has a total helicity ( $\alpha$ ,  $3_{10}$ ) of 31%, whereas p53pSer15 is helical for only 4% of the simulation. The helix observed in the unphosphorylated peptide spans residues Pro12-Thr18. An  $i, i + 4$  interaction known to stabilize helices is observed between the backbone of residues Glu11 and Ser15 of p53 for 53% of the simulation (Figure 4A). Additional  $i, i + 4$  interactions observed include the backbone of Pro12 and Gln16 (44%), and the backbone of Leu14 with the sidechain of Thr18 (32%).

In addition to intramolecular interactions, we also examined intermolecular interactions between the peptides and CK1 $\delta$  to look for interactions that stabilize peptide binding. The sidechain of Ser15 in p53 interacts with Glu90 and Tyr179, whereas in p53pSer15, it almost exclusively interacts and forms a salt bridge with Arg178 which is located in the positively charged pocket of the kinase (Figures 4B and S2). Arg178 interacts with Glu17 in p53, while Glu17 also interacts with Lys224, occasionally forming salt



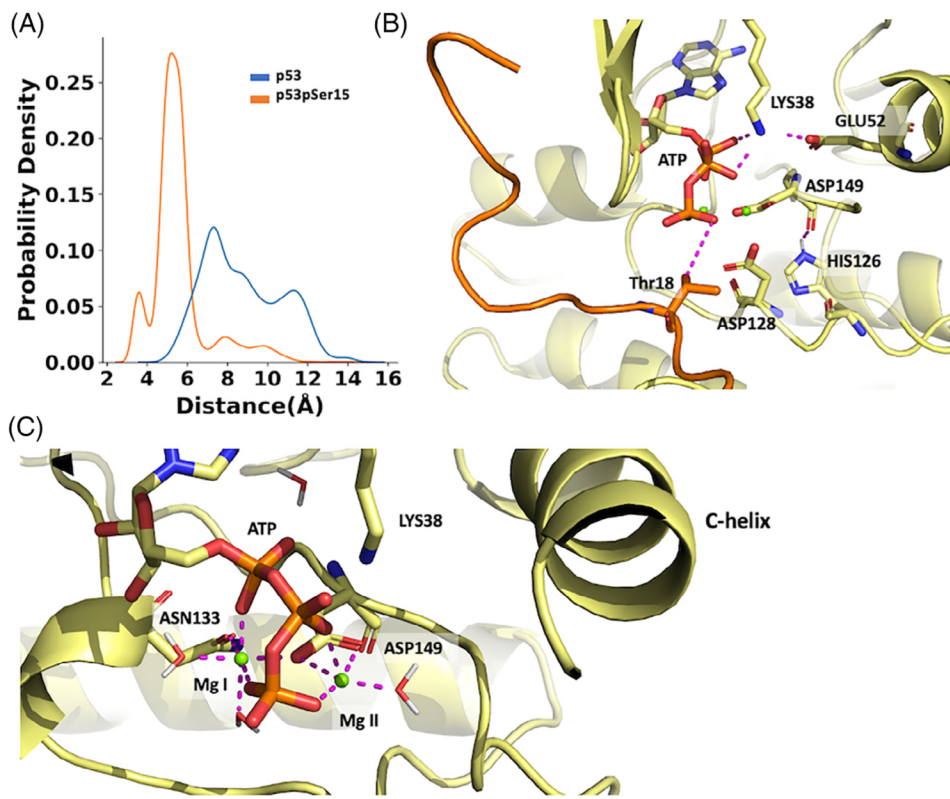


**FIGURE 5** Thr18 is closer to the  $\gamma$ -phosphate of adenosine triphosphate (ATP) when Ser15 is phosphorylated. (A) Probability density distribution of the distance from the side chain -OH of Thr18 to the  $\gamma$ -phosphate of ATP. p53 and p53pSer15 peptides are colored in blue and orange, respectively. (B) Detailed interactions within the ATP binding pocket in the active kinase state. (C) Coordination of the 2 Mg $^{2+}$  ions in the catalytic pocket of casein kinase 1 $\delta$  (CK1 $\delta$ ). CK1 $\delta$  is shown in yellow, the p53pSer15 peptide is shown in orange and the Mg $^{2+}$  ions are shown as green spheres.

bridges (Figure 4A). p53pSer15 samples a high population of disordered conformations and the phosphorylated, and negatively charged residues of the peptide are stabilized mainly by interactions with Arg178, Lys 221, and Lys 224 within the positively charged pocket of CK1 $\delta$  (Figure 4B). Arg222 of CK1 $\delta$  forms H-bonds and in some cases salt bridges with Asp21 of p53 in both unphosphorylated and phosphorylated systems (Figure S3A,B). Arg98 is another positively charged residue near the catalytic pocket whose side chain only occasionally interacts with Glu11 in the p53pSer15 peptide due to the presence of several basic residues, but consistently forms a salt bridge with the side chain of Glu11 of p53 (Figure 4A). The sidechain of Lys130 which is also located near the catalytic pocket forms H-bonds with the backbone of Gln16 of p53pSer15, but this interaction is not observed in the p53 peptide (Figure S4). At the catalytic site, CK1 $\delta$  has a nonpolar patch compatible with a hydrophobic amino acid.<sup>34</sup> This accommodates Phe19 of p53pSer15, being adjacent to Thr18, which in turn interacts with Gly175 of the kinase in both complexes (Figure S5A,B).

### 3.5 | Effect of Ser15 phosphorylation on the structure of CK1 $\delta$

The introduction of a negatively charged phosphate group at Ser15 in the positively charged pocket of CK1 $\delta$  also induces structural changes in the kinase. More specifically, the positively charged pocket of CK1 $\delta$  closes due to the electrostatic attraction between the positively

charged amino acids of the binding pocket and the negatively charged amino acids of the peptide (Figure 4D). This process is instigated by the presence of the negatively charged phosphate. Its absence in p53 results in the pocket remaining open (Figure 4C). Additionally, the p-loop in the phosphorylated complex undergoes a conformational change that is accompanied by interactions between Ser19 and the backbone of Thr18 which also contributes to stabilizing the residue in a state that is appropriate for receiving the incoming phosphate from ATP (Figure S6). On the contrary, in the p53 complex, the side chain of Thr18 is not in the correct orientation for the phospho-transfer reaction to take place and is further away compared with its location in p53pSer15.

### 3.6 | Phosphorylation at Ser15 brings p53 Thr18 closer to ATP

Next, we calculated the distance between the  $\gamma$ -phosphate of ATP and the side-chain oxygen of Thr18 for both p53 and p53pSer15 complexes. The distance for p53 spans a broad range between 4 and 16 Å, whereas for p53pSer15 the range is between 2 and 14 Å with a major peak at 5 Å (Figure 5A). The negatively charged phosphate in p53pSer15 and the accompanying disorder in the peptide clearly enable Thr18 to be placed close to and in the correct orientation relative to ATP for phosphate transfer.

Possible mechanisms of phosphate transfer include the base-assisted mechanism (dissociative mechanism), and the substrate-assisted mechanism (associative mechanism).<sup>55</sup> During the base-

**TABLE 1** Contributions made by van der Waals, electrostatic, and solvation energy components to the total estimated MMPBSA binding energy between p53/p53pSer15 peptides and CK1 $\delta$  from aMD simulations

	vdW <sup>a</sup> (kcal/mol)	EEL <sup>b</sup> (kcal/mol)	EPB <sup>c</sup> (kcal/mol)	Enpolar <sup>d</sup> (kcal/mol)	$\Delta G_{\text{sol}}^{\text{e}}$ (kcal/mol)	$\Delta G_{\text{total}}^{\text{f}}$ (kcal/mol)
p53	-83.8	-839.3	858.6	-15.1	843.4	-79.7 ( $\pm 1.2$ )
p53pSer15	-89.0	-1409.9	1417.7	-15.4	1402.2	-96.6 ( $\pm 1.1$ )

Abbreviations: CK1 $\delta$ , casein kinase 1 $\delta$ ; MD, molecular dynamics; MMPBSA, molecular mechanics Poisson Boltzmann surface area.

<sup>a</sup>van der Waals contribution.

<sup>b</sup>Electrostatic energy.

<sup>c</sup>Polar contribution to the solvation free energy.

<sup>d</sup>Nonpolar contribution to the solvation free energy.

<sup>e</sup>Solvation free energy = EPB + Enpolar.

<sup>f</sup>Final estimated binding free energy with standard error of mean.

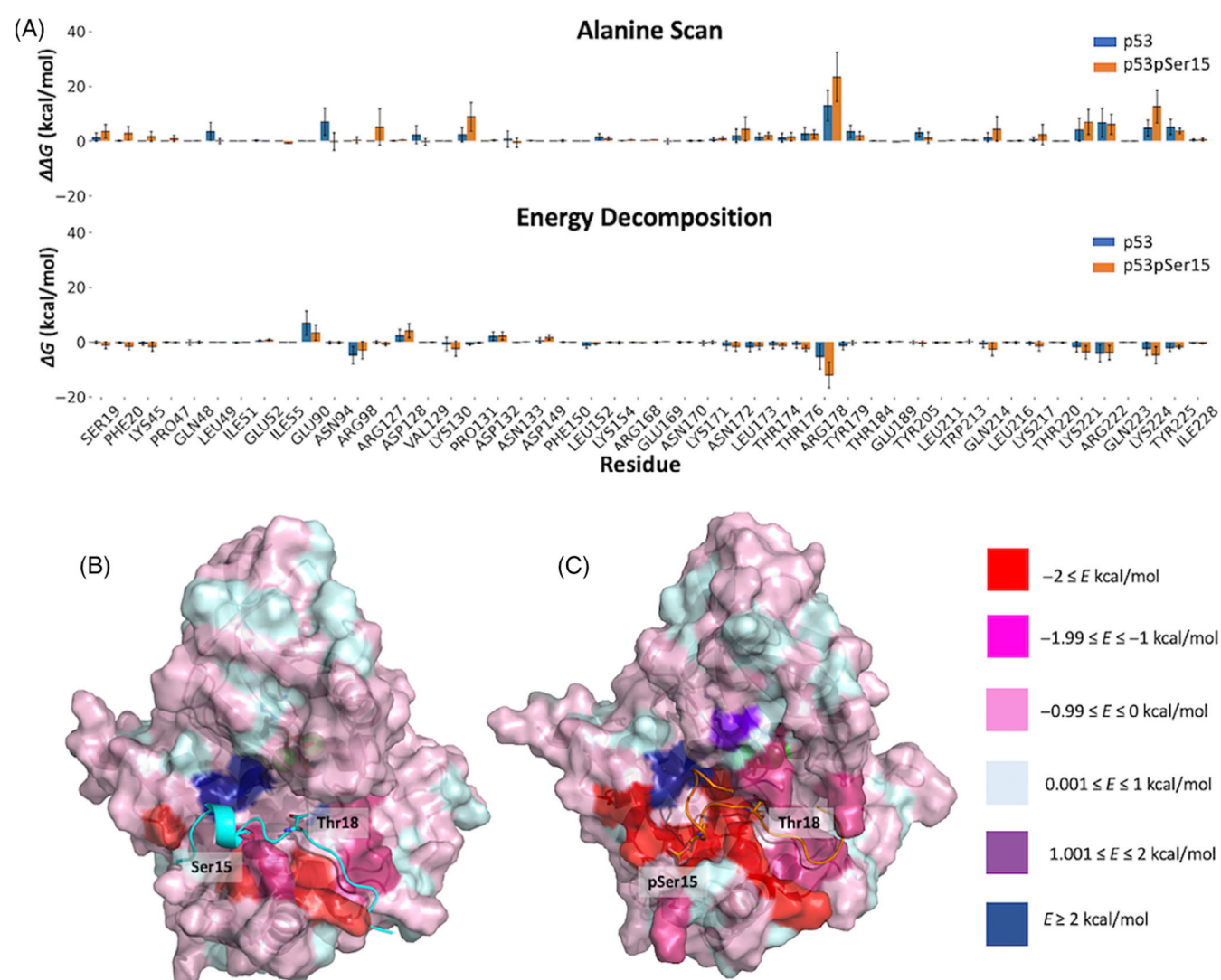


**FIGURE 6** Individual energy contributions of casein kinase 1 $\delta$  (CK1 $\delta$ ) residues to overall binding. (A) Per residue energy decomposition and alanine scan of CK1 $\delta$  residues within 6 Å from peptides. CK1 $\delta$  in complex with p53 is colored in blue and CK1 $\delta$  in complex with p53pSer15 is colored in orange. (B,C) Surface of CK1 $\delta$  in complex with p53 (cyan) and p53pSer15 (orange). The surface of CK1 $\delta$  is color-coded based on the residue energy contributions from energy decomposition calculations.

assisted mechanism of phosphate transfer, nucleophilic Thr18 would get deprotonated by Asp128 and become even more nucleophilic. In the substrate-based mechanism, the hydroxyl proton of Thr18 would

be transferred to a  $\gamma$ -PO<sub>4</sub> oxygen. Asp128 belongs to the conserved HRD (His-Arg-Asp) kinase motif, known to interact with the substrate in the active kinase state.<sup>56</sup> As part of the phosphate transfer



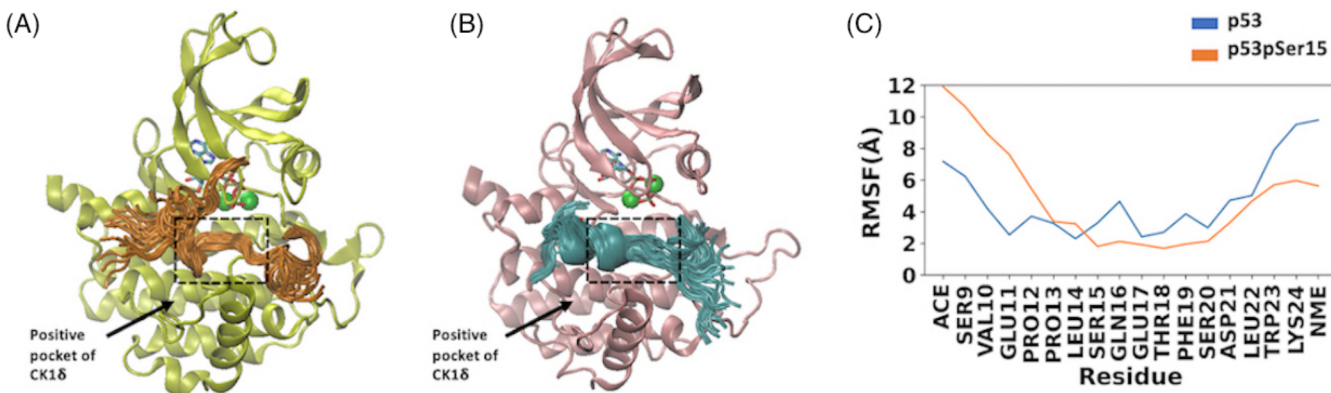


**FIGURE 7** Fuzzy complexes of p53 and p53pSer15 peptides with casein kinase 1 $\delta$  (CK1 $\delta$ ). (A) Representative conformations of the p53pSer15 peptide (orange) bound to CK1 $\delta$  (yellow), resembling a flanking fuzzy complex. (B) Representative conformations of the p53 peptide (cyan) bound to CK1 $\delta$  (pink), resembling a flanking fuzzy complex. For panels (A,B) Mg $^{2+}$  ions are shown as green spheres and adenosine triphosphate is shown in sticks. The dashed line boxes focus on the location of residues Ser15–Ser20. (C) Root mean square fluctuation (RMSF) per residue for p53 (blue) and p53pser15 (orange) peptides.

mechanism, Lys38 interacts with  $\alpha$ - and  $\beta$ -phosphate oxygens of ATP, while also interacting with Glu52 (Figure 5B). Asp149 is part of the conserved DFG (Asp-Phe-Gly) motif and it binds to the Mg $^{2+}$  ion that directly interacts with an oxygen atom of the  $\beta$ -phosphate of ATP. In the active kinase state Asp149 also interacts with the His from the HRD motif, in this case His126 (Figure 5B). The first Mg $^{2+}$  ion interacts with two nonbinding oxygen atoms from the  $\alpha$ - and  $\gamma$ -phosphates of ATP, Asp149, Asn133, and two water molecules. The second Mg $^{2+}$  ion is coordinated by a  $\beta$ - and a  $\gamma$ -phosphate oxygen of ATP, a bidentate coordination with Asp149, and a water molecule (Figure 5C). A study by Recabarren et al.<sup>55</sup> on CDK2, another Ser/Thr kinase describes the Mg $^{2+}$  coordination states and phosphate transfer mechanism in more detail. Although our models could not unambiguously differentiate between the phosphate transfer mechanisms at play in the simulations, recent studies suggest that the base-assisted mechanism is usually favored.<sup>55,57,58</sup>

### 3.7 | Phosphorylated p53 peptide binds more strongly to CK1 $\delta$

Binding energy calculations on the MD trajectories were carried out using the MMPBSA method to characterize the energetics associated with the binding of p53 and p53pSer15 peptides to CK1 $\delta$ . The binding of p53pSer15 ( $\Delta G = -96.6$  kcal/mol) to CK1 $\delta$  was stronger than p53 ( $\Delta G = -79.7$  kcal/mol; Table 1). This is driven by greater van der Waals contributions that arise from the more extensive interactions between the extended conformation of p53pSer15 compared with the ordered conformation of p53, and by the electrostatic attraction between the positively charged pocket of CK1 $\delta$  and the negatively charged phosphate of p53pSer15.

Decomposing the total energetics into contributions by residues revealed that Arg98, Arg178, Lys221, Arg222, and Lys224 make significant contributions to binding in both the p53 and p53pSer15 CK1 $\delta$

complexes (Figure 6A–C). However, the contributions of Arg178, Lys221, and Lys224 are higher in the complex with p53pSer15 due to the presence of negatively charged phosphoserine. Other residues that contribute to binding are Lys130, Thr176, and Gln214 in the p53pSer15 complex and Tyr225 mainly in the p53 complex.

The individual contributions of different amino acids were also measured by performing alanine scanning. Alanine scanning was carried out for the p53 and p53pSer15 CK1 $\delta$  complexes for all kinase residues within 6 Å of the peptides. All residues were mutated to Ala with the exception of Gly. The energy contribution,  $\Delta\Delta G$ , of the residues agreed with energy decomposition per residue calculations. In both methods, the positively charged residues in the catalytic pocket that contributed significantly to binding were Arg98, Lys130 (p53pSer15), Arg178, Lys221, Arg222, and Lys224 (Figure 6A).

### 3.8 | Fuzzy binding of p53pSer15 peptide to CK1 $\delta$

The binding of p53pSer15 to CK1 $\delta$  resembles a fuzzy complex since it retains conformational variability even after binding. CK1 $\delta$  uses the pSer/pThr-X-X-Ser/Thr motif in the linker region of the p53pSer15 peptide to recognize and bind to it, while it retains disordered flanking segments (Figure 7A). The linker region of p53pSer15 loses its helicity upon phosphorylation but binds more strongly to CK1 $\delta$  due to electrostatic interactions that take place between the phosphorylated peptide and the kinase. The p53 peptide also binds to CK1 $\delta$  and forms a fuzzy complex but interacts less strongly compared with the p53pSer15 peptide and samples different conformations (Figure 7B). RMSF was used to measure the average fluctuation per residue over time for the p53pSer15 and p53 peptides (Figure 7C). Residues Ser15–Ser20 had lower RMSF values in the phosphorylated peptide. This suggests that the p53pSer15 peptide interacts more strongly with CK1 $\delta$  and is more tightly bound compared with the unphosphorylated p53 peptide. The differences in fluctuations can be seen

in Figure 7A,B where several overlapping conformations of each peptide are shown.

### 3.9 | Impact of CK1 $\delta$ mutations on p53 and p53pSer15 peptide binding

CK1 $\delta$  residues Arg98, Lys130, Arg178, Lys221, Arg222, and Lys224 were mutated based on the results of alanine scanning. Individual aMD simulations for each mutation were carried out to test whether each residue's mutation to Ala would affect the peptide binding to CK1 $\delta$ . Mutation simulations significantly affected the binding of p53 to the kinase while they had minimal effect on the binding of p53pSer15. Residue-level decomposition analysis was carried out for each mutation and showed that the basic residues of CK1 $\delta$  responsible for binding to the p53pSer15 peptide individually contribute significantly less when mutated to Ala; upon mutation the attenuation in interactions is compensated by neighboring positively charged residues. For example, when Arg178 is mutated to Ala, Lys224 has a larger energy contribution compared with the WT (Figure S7A). This pattern is also observed in simulations of mutations of K224A, whose interactions are compensated by Arg178 and Lys217 (Figure S7B). However, this is not the case in the p53 complex, where there is not enough negative charge and when one residue from the positively charged pocket is mutated the electrostatic interactions of the N-terminus with the slightly less positive pocket are not strong enough to hold the peptide in place; indeed, in none of the mutations in CK1 $\delta$  does unphosphorylated p53 stay in the binding pocket.

## 4 | DISCUSSION

In this work, we used accelerated MD in an effort to understand why the p53 activating phosphorylation of Thr18 in TAD by CK1 $\delta$  requires Ser15 phosphorylation as a prerequisite. We first studied the conformational dynamics of p53 and p53pSer15 peptides in their free forms and then in complex with CK1 $\delta$ . MD simulations revealed that phosphorylation at Ser15 perturbs the structure of p53 peptide significantly when bound to CK1 $\delta$ , while the structure of p53pSer15 remains partially helical when free in solution. On the other hand, p53 is mostly helical in its free form (between residues Leu14 and Lys24) and remains partly helical in the bound state (Pro12-Thr18). This is in agreement with solution NMR studies which reported that free p53 TAD1 is helical between residues Thr18 to Leu26.<sup>58,59</sup> p53pSer15 lacks helical structure when bound to CK1 $\delta$  and is localized closer to ATP compared with p53. The disordered nature of p53pSer15 increases its flexibility which enables it to bind tighter to CK1 $\delta$ . Systems that are electrostatically driven are likely dominated by induced fit mechanisms such as the positively charged pocket of CK1 $\delta$  and negatively charged pSer15 of the p53 peptide. Energetic analysis identified CK1 $\delta$  residues Arg98, Lys130, Arg178, Lys221, and Arg222, Lys224 important for binding to p53pSer15. Arg178 and Lys224 had been speculated earlier to be involved in enabling interactions with acidic substrates.<sup>60</sup>

The conservation of the positively charged residues of the CK1 $\delta$  pocket was examined across the CK1 family (not including its closest relatives tau tubulin kinases 1 and 2 and the vaccinia-related kinases 1–3).<sup>21</sup> Arg98, Lys130, and Arg178 are fully conserved across the CK1 subfamily. Arg222 and Lys224 are partially conserved (Figure S8A). Lys221 is not conserved across the CK1 subfamily (Figure S8A). We also investigated the conservation of these residues across species available in UniProt.<sup>61</sup> All six positively charged residues in human CK1 $\delta$  are fully conserved in mouse, rat, cattle, orangutan, African clawed frog, and Western clawed frog (Figure S8B). This clearly suggests that the sequential phosphorylation process with Ser15 getting phosphorylated first is likely conserved in evolution.

The motif pSer/pThr-X-X-(X)-Ser/Thr is the canonical consensus sequence for CK1 $\delta$  substrates.<sup>22,23</sup> It is clear that the negatively charged phosphate at the –3 position is sequestered by a cationic patch on the kinase. There are also substrates that carry this motif, but with a negative charge in the form of Asp/Glu amino acids at the –3 position as these too can be sequestered by the cationic patch, albeit less strongly, because of the trigonal planar disposition of the carboxyl group and the less negative charge compared with the tetrahedral disposition and charge of the phosphate group.<sup>62</sup> Substrates of CK1 $\delta$  include TA�63 $\alpha$ , where CK1 $\delta$  phosphorylates four residues in a sequential manner having a Ser residue at the –3 position, with each newly phosphorylated residue acting as the priming site for the following phosphorylation event.<sup>32</sup> Additionally, CK1 $\delta$  phosphorylates two Ser residues on FOXO1a, with a “priming” phosphate on Ser at the –3 position.<sup>63</sup> CK1 $\delta$  also phosphorylates multiple Ser residues in the acidic domain of MDM2 using acidic amino acids as priming residues.<sup>64</sup> BID contains a cluster of acidic residues upstream of its Ser residue phosphorylated by CK1, and once phosphorylated can serve as the priming residue for additional phosphorylation events.<sup>65,66</sup> Furthermore, YAP a protein increasingly recognized for its role in health/disease that is part of the HIPPO pathway (YAP/TEAD interaction), gets phosphorylated by Lats on Ser381, which provides a priming signal for CK1 $\delta$  to phosphorylate Ser384 and Ser387.<sup>67</sup> It is interesting that the associated YAP sequence is <sup>379</sup>D**E**<sup>380</sup>T**D****S****G****L****S****M**<sup>388</sup> and phosphorylation of Ser381 would result in a long-negative potential subtended by Asp, Glu, and pSer, that likely translates into higher affinity of the peptide. Detailed lists of CK1 $\delta$  substrates can be found in comprehensive reviews on the CK1 family of kinases.<sup>21,66</sup> In addition, it also appears that a hydrophobic residue located at the +1 or +2 position may serve to further anchor the peptide by interacting with a hydrophobic patch on CK1 $\delta$  that includes Gly175 (this residue and the region are evolutionarily conserved in the CK1 family; Figure S8). For example, in p53 the residue interacting with the hydrophobic patch of CK1 $\delta$  is Phe19, in FOXO1 is Gly326 (phosphorylation sites are S322 and S325), and in YAP Ser384 and Ser387 are followed by hydrophobic residues Gly385 and Leu388, respectively. Indeed, in the case of p53, the contribution of Phe19 to the total interaction energy is approximately –4.9 kcal/mol in the phosphorylated state and approximately –3.5 kcal/mol in the unphosphorylated state. The higher stability in the phosphorylated state suggests that this hydrophobic interaction may be a second anchor point, together with the acidic region, to hold the substrate for phosphorylation.



IDPs such as p53 TAD1, are complex systems and often have multiple binding partners. The structure of IDPs fluctuates as they bind to different partners. TAD1 of p53 has a helical conformation when bound to MDM2, and it was found that free p53 TAD1 peptides retain their helicity in solution and bind to MDM2 through conformational selection.<sup>69</sup> Our observations on the helicity of free p53 TAD1 peptides from residue Gln16 onwards are consistent with the study of Yadahalli et al.<sup>69</sup> Our molecular modeling studies showed that p53 TAD1 also partially retains its helicity when bound to CK1 $\delta$ . However, p53 TAD1 loses helicity upon Ser15 phosphorylation, and its binding mechanism appears to be induced fit.

In summary, phosphorylation of Thr18 in p53 TAD1 by CK1 $\delta$  requires Ser15 to be phosphorylated first to enable sequestration of the p53pSer15 peptide to the positively charged pocket of CK1 $\delta$ . This interaction is mediated by a network of conserved positive charges in CK1 $\delta$  and the negatively charged p53pSer15 peptide. Phosphorylated Ser15 serves as the initial anchor point, which enables the remaining peptide to morph itself onto the surface of CK1 $\delta$ , forming a fuzzy complex. This places the Thr18 hydroxyl group within close proximity and in the right orientation relative to the  $\gamma$ -phosphate of ATP for efficient transfer of the phosphate to Thr18. Our models suggest that a hydrophobic interaction at the +1 position of Thr18 may further contribute to anchoring the peptide. The combination of these results along with additional experimental studies focusing on p53 TAD1 and its binding to various partners could further decipher the activation mechanism of p53 by multisite phosphorylation which could be exploited for drug discovery.

## ACKNOWLEDGMENTS

The authors would like to acknowledge the University of Manchester and Agency for Science, Technology, and Research (A\*STAR) for funding as well as the National Supercomputing Centre (NSCC), Singapore for computing facilities. STN thanks Stephen Fox and Pietro Aronica for support and guidance.

## FUNDING INFORMATION

This work was supported by a joint PhD studentship from the University of Manchester and A\*STAR Singapore.

## CONFLICT OF INTERESTS

Chandra S. Verma and Srinivasaraghavan Kannan are founders of Sinopsee Therapeutics and Aplomex.

## DATA AVAILABILITY STATEMENT

All simulation data can be provided upon request.

## ORCID

Sonia T. Nicolaou  <https://orcid.org/0000-0001-6849-6872>

Srinivasaraghavan Kannan  <https://orcid.org/0000-0002-9539-5249>

Jim Warwicker  <https://orcid.org/0000-0002-1302-0815>

Chandra S. Verma  <https://orcid.org/0000-0003-0733-9798>

## REFERENCES

- Wright PE, Dyson HJ. Intrinsically unstructured proteins: re-assessing the protein structure-function paradigm. *J Mol Biol*. 1999;293(2):321-331.
- Tompa P. Intrinsically unstructured proteins. *Trends Biochem Sci*. 2002;27:527-533.
- Uversky VN, Gillespie JR, Fink AL. Why are “natively unfolded” proteins unstructured under physiologic conditions? *Proteins*. 2000;41(3):415-427.
- Dunker AK, Lawson JD, Brown CJ, et al. Intrinsically disordered protein. *J Mol Graph Model*. 2001;19(1):26-59.
- Dyson HJ, Wright PE. Intrinsically unstructured proteins and their functions. *Nat Rev Mol Cell Biol*. 2005;6:197-208.
- Bah A, Forman-Kay JD. Modulation of intrinsically disordered protein function by post-translational modifications. *J Biol Chem*. 2016;291(13):6696-6705.
- Iakoucheva LM, Radivojac P, Brown CJ, et al. The importance of intrinsic disorder for protein phosphorylation. *Nucleic Acids Res*. 2004;32(3):1037-1049.
- Künzel N, Helms V. How phosphorylation of peptides affects their interaction with 14-3-3 $\eta$  domains. *Proteins*. 2022;90(2):351-362.
- Zuckerman V, Lenos K, Popowicz GM, et al. C-Abl phosphorylates Hdmx and regulates its interaction with p53. *J Biol Chem*. 2009;284(6):4031-4039.
- Gnad F, Forner F, Zielinska DF, Birney E, Gunawardena J, Mann M. Evolutionary constraints of phosphorylation in eukaryotes, prokaryotes, and mitochondria. *Mol Cell Proteomics*. 2010;9(12):2642-2653.
- Krois AS, Dyson HJ, Wright PE. Long-range regulation of p53 DNA binding by its intrinsically disordered N-terminal transactivation domain. *Proc Natl Acad Sci U S A*. 2018;115(48):E11302-E11310.
- Krois AS, Ferreon JC, Martinez-Yamout MA, Dyson HJ, Wright PE. Recognition of the disordered p53 transactivation domain by the transcriptional adapter zinc finger domains of CREB-binding protein. *Proc Natl Acad Sci U S A*. 2016;113(13):E1853-E1862.
- Kruse JP, Gu W. Modes of p53 regulation. *Cell*. 2009;137(4):609-622.
- Brooks CL, Gu W. p53 ubiquitination: Mdm2 and beyond. *Mol Cell*. 2006;21(3):307-315.
- Michael D, Oren M. The p53-Mdm2 module and the ubiquitin system. *Semin Cancer Biol*. 2003;13(1):49-58.
- Lee CW, Ferreon JC, Ferreon ACM, Arai M, Wright PE. Graded enhancement of p53 binding to CREB-binding protein (CBP) by multisite phosphorylation. *Proc Natl Acad Sci U S A*. 2010;107(45):19290-19295.
- MacLaine NJ, Hupp TR. The regulation of p53 by phosphorylation: a model for how distinct signals integrate into the p53 pathway. *Aging*. 2009;1(5):490-502.
- Chen H-F, Luo R. Binding Induced Folding in p53-MDM2 Complex. *J Am Chem Soc*. 2007;129(10):2930-2937.
- Sakaguchi K, Si S, Higashimoto Y, Roy S, Anderson CW, Appella E. Damage-mediated phosphorylation of human p53 threonine 18 through a cascade mediated by a casein 1-like kinase. Effect on MDM2 binding. *J Biol Chem*. 2000;275(13):9278-9283.
- Dumaz N, Milne DM, Meek DW. Protein kinase CK1 is a p53-threonine 18 kinase which requires prior phosphorylation of serine 15. *FEBS Lett*. 1999;463(3):312-316.
- Knippschild U, Krüger M, Richter J, et al. The CK1 family: contribution to cellular stress response and its role in carcinogenesis. *Front Oncol*. 2014;4:96.
- Flotow H, Graves PR, Wang A, Fiol CJ, Roeske RW, Roach PJ. Phosphate groups as substrate determinants for casein kinase I action. *J Biol Chem*. 1990;265(24):14264-14269.
- Songyang Z, Lu KP, Kwon YT, et al. A structural basis for substrate specificities of protein Ser/Thr kinases: primary sequence preference of casein kinases I and II, NIMA, phosphoprotein kinase, calmodulin-dependent kinase II, CDK5, and Erk1. *Mol Cell Biol*. 1996;16(11):6486-6493.



24. Dyson HJ, Wright PE. Coupling of folding and binding for unstructured proteins. *Curr Opin Struct Biol.* 2002;12:54-60.
25. Mollica L, Bessa LM, Hanouille X, Jensen MR, Blackledge M, Schneider R. Binding mechanisms of intrinsically disordered proteins: theory, simulation, and experiment. *Front Mol Biosci.* 2016;3:52.
26. Chen HF. Molecular dynamics simulation of phosphorylated KID post-translational modification. *PLoS One.* 2009;4(8):e6516.
27. Turjanski AG, Gutkind JS, Best RB, Hummer G. Binding-induced folding of a natively unstructured transcription factor. *PLoS Comput Biol.* 2008;4(4):e1000060.
28. Tompa P, Fuxreiter M. Fuzzy complexes: polymorphism and structural disorder in protein-protein interactions. *Trends Biochem Sci.* 2008;33(1):2-8.
29. Fuxreiter M, Tompa P. Fuzzy complexes: a more stochastic view of protein function. *Adv Exp Med Biol.* 2012;725:1-14.
30. Hamelberg D, Mongan J, McCammon JA. Accelerated molecular dynamics: a promising and efficient simulation method for biomolecules. *J Chem Phys.* 2004;120(24):11919-11929.
31. Case DA, Ben-Shalom IY, Brozell SR, et al. AMBER 2019. University of California; 2019.
32. Gebel J, Tuppi M, Chaikuaad A, et al. p63 uses a switch-like mechanism to set the threshold for induction of apoptosis. *Nat Chem Biol.* 2020;16(10):1078-1086.
33. Berman HM. The protein data bank. *Nucleic Acids Res.* 2000;28(1):235-242.
34. Das A, Gerlits O, Parks JM, Langan P, Kovalevsky A, Heller WT. Protein kinase a catalytic subunit primed for action: time-lapse crystallography of Michaelis complex formation. *Structure.* 2015;23(12):2331-2340.
35. DeLano WL. *The PyMOL Molecular Graphics System.* De Lano Scientific; 2002.
36. Šali A, Blundell TL. Comparative protein modelling by satisfaction of spatial restraints. *J Mol Biol.* 1993;234(3):779-815.
37. Williams CJ, Headd JJ, Moriarty NW, et al. MolProbity: more and better reference data for improved all-atom structure validation. *Protein Sci.* 2018;27(1):293-315.
38. Jurrus E, Engel D, Star K, et al. Improvements to the APBS biomolecular solvation software suite. *Protein Sci.* 2018;27(1):112-128.
39. Word JM, Lovell SC, Labean TH, et al. Visualizing and quantifying molecular goodness-of-fit: small-probe contact dots with explicit hydrogen atoms. *J Mol Biol.* 1999;285(4):1711-1733.
40. Juraszek J, Bolhuis PG. Sampling the multiple folding mechanisms of Trp-cage in explicit solvent. *Proc Natl Acad Sci U S A.* 2006;103(43):15859-15864.
41. Case DA, Darden TA, Cheatham III TE, et al. AMBER 2011. University of California; 2010.
42. Maier JA, Martinez C, Kasavajhala K, Wickstrom L, Hauser KE, Simmerling C. ff14SB: improving the accuracy of protein side chain and backbone parameters from ff99SB. *J Chem Theory Comput.* 2015;11(8):3696-3713.
43. Case DA, Ben-Shalom IY, Brozell SR, et al. AMBER 2018. University of California; 2018.
44. Jorgensen WL, Chandrasekhar J, Madura JD, Impey RW, Klein ML. Comparison of simple potential functions for simulating liquid water. *J Chem Phys.* 1983;79(2):926-935.
45. Kannan S, Lane DP, Verma CS. Long range recognition and selection in IDPs: the interactions of the C-terminus of p53. *Sci Rep.* 2016;6:26750.
46. Darden T, York D, Pedersen L. Particle mesh Ewald: an N-log (N) method for Ewald sums in large systems. *J Chem Phys.* 1993;98(12):10089-10092.
47. Van Gunsteren WF, Berendsen HJC. Algorithms for macromolecular dynamics and constraintdynamics. *Mol Phys.* 1977;34(5):1311-1327.
48. Homeyer N, Horn AHC, Lanig H, Sticht H. AMBER force-field parameters for phosphorylated amino acids in different protonation states: phosphoserine, phosphothreonine, phosphotyrosine, and phosphohistidine. *J Mol Model.* 2006;12(3):281-289.
49. Homeyer N, Gohlke H. Free energy calculations by the molecular mechanics Poisson-Boltzmann surface area method. *Mol Inform.* 2012;31(2):114-122.
50. Hou T, Wang J, Li Y, Wang W. Assessing the performance of the molecular mechanics/Poisson Boltzmann surface area and molecular mechanics/generalized born surface area methods. II. The accuracy of ranking poses generated from docking. *J Comput Chem.* 2011;32(5):866-877.
51. Roe DR, Cheatham TE. PTRAJ and CPPTRAJ: software for processing and analysis of molecular dynamics trajectory data. *J Chem Theory Comput.* 2013;9(7):3084-3095.
52. Kabsch W, Sander C. Dictionary of protein secondary structure: pattern recognition of hydrogen-bonded and geometrical features. *Bio-polymers.* 1983;22(12):2577-2637.
53. Humphrey W, Dalke A, Schulten K. VMD: visual molecular dynamics. *J Mol Graph.* 1996;14(1):33-38.
54. Kussie PH, Gorina S, Marechal V, et al. Structure of the MDM2 Onco-protein bound to the p53 tumor suppressor transactivation domain. *Science.* 1996;274(5289):948-953.
55. Recabarren R, Zinovjev K, Tuñón I, Alzate-Morales J. How a second Mg<sup>2+</sup>ion affects the phosphoryl-transfer mechanism in a protein kinase: a computational study. *ACS Catal.* 2021;11(1):169-183.
56. Modi V, Dunbrack RL. Defining a new nomenclature for the structures of active and inactive kinases. *Proc Natl Acad Sci U S A.* 2019;116(14):6818-6827.
57. Recabarren R, Osorio EH, Caballero J, Tuñón I, Alzate-Morales JH. Mechanistic insights into the phosphoryl transfer reaction in cyclin-dependent kinase 2: a QM/MM study. *PLoS One.* 2019;14(9):e0215793.
58. Murillo-López J, Zinovjev K, Pereira H, et al. Studying the phosphoryl transfer mechanism of the *E. coli* phosphofructokinase-2: from X-ray structure to quantum mechanics/molecular mechanics simulations. *Chem Sci.* 2019;10(10):2882-2892.
59. Lee H, Mok KH, Muhandiram R, et al. Local structural elements in the mostly unstructured transcriptional activation domain of human p53. *J Biol Chem.* 2000;275(38):29426-29432.
60. Song D, Liu H, Luo R, Chen H-F. Environment-specific force field for intrinsically disordered and ordered proteins. *J Chem Inf Model.* 2020;60:2257-2267.
61. Xu P, lanes C, Gartner F, et al. Structure, regulation, and (patho-)physiological functions of the stress-induced protein kinase CK1 delta (CSNK1D). *Gene.* 2019;715:144005.
62. Bateman A. UniProt: a worldwide hub of protein knowledge. *Nucleic Acids Res.* 2019;47(D1):D506-D515.
63. Ng YW, Raghunathan D, Chan PM, et al. Why an A-loop phosphomimetic fails to activate PAK1: understanding an inaccessible kinase state by molecular dynamics simulations. *Structure.* 2010;18(7):879-890.
64. Rena G, Bain J, Elliott M, Cohen P. D4476, a cell-permeant inhibitor of CK1, suppresses the site-specific phosphorylation and nuclear exclusion of FOXO1a. *EMBO Rep.* 2004;5(1):60-65.
65. Winter M, Milne D, Dias S, et al. Protein kinase CK1δ phosphorylates key sites in the acidic domain of murine double-minute clone 2 protein (MDM2) that regulate p53 turnover. *Biochemistry.* 2004;43(51):16356-16364.
66. Desagher S, Osen-Sand A, Montessuit S, et al. Phosphorylation of bid by casein kinases I and II regulates its cleavage by caspase 8. *Mol Cell.* 2001;8(3):601-611.
67. Schittek B, Sinnberg T. Biological functions of casein kinase 1 isoforms and putative roles in tumorigenesis. *Mol Cancer.* 2014;13:231.
68. Zhao B, Li L, Tumaneng K, Wang CY, Guan KL. A coordinated phosphorylation by Lats and CK1 regulates YAP stability through SCF(beta-TRCP). *Genes Dev.* 2010;24(1):72-85.



69. Yadahalli S, Li J, Lane DP, Gosavi S, Verma CS. Characterizing the conformational landscape of MDM2-binding p53 peptides using molecular dynamics simulations. *Sci Rep.* 2017;7(1):15600.

#### SUPPORTING INFORMATION

Additional supporting information can be found online in the Supporting Information section at the end of this article.

**How to cite this article:** Nicolaou ST, Kannan S, Warwicker J, Verma CS. Activation of p53: How phosphorylated Ser15 triggers sequential phosphorylation of p53 at Thr18 by CK1δ. *Proteins.* 2022;90(12):2009–2022. doi:[10.1002/prot.26393](https://doi.org/10.1002/prot.26393)



